Establishment of two ovarian cancer orthotopic xenograft mouse models for *in vivo* imaging: A comparative study

JING GUO[1*], JING CAI[1*], YUNXIA ZHANG[1], YAPEI ZHU[2], PING YANG[3] and ZEHUA WANG[1]

[1]Department of Obstetrics and Gynecology, Union Hospital, Tongji Medical College, Huazhong University of Science and Technology, Wuhan 430022; [2]Department of Obstetrics and Gynecology, Peking Union Medical College Hospital, Beijing 100730; [3]Department of Obstetrics and Gynecology, First Affiliated Hospital, School of Medicine, Shihezi University, Shihezi, Xinjiang 832008, P.R. China

Received June 22, 2017; Accepted July 12, 2017

DOI: 10.3892/ijo.2017.4115

Abstract. Orthotopic tumor animal models are optimal for preclinical research of novel therapeutic interventions. The aim of the present study was to compare two types of ovarian cancer orthotopic xenograft (OCOX) mouse models, i.e. cellular orthotopic injection (COI) and surgical orthotopic implantation (SOI), regarding xenograft formation rate, *in vivo* imaging, tumor growth and metastasis, and tumor microenvironment. The tumor formation and progression were monitored by bioluminescent *in vivo* imaging. Cell proliferation and migration abilities were detected by EdU and scratch assays, respectively. Expression of α-SMA, CD34, MMP2, MMP9, vimentin, E-cadherin and Ki67 in tumor samples were detected by immunohistochemistry. As a result, we successfully established COI- and SOI-OCOX mouse models using ovarian cancer cell lines ES2 and SKOV3. The tumor formation rate in the COI and SOI models were 87.5 and 100%, respectively. Suspected tumor cell leakage occurred in 37.5% of the COI models. The SOI xenografts grew faster, held larger primary tumors, and were more metastatic than the COI xenografts. The migration and proliferation properties of the cells that generated SOI xenografts were significantly starker than those deriving COI xenografts *in vitro*. The tumor cells in SOI xenografts exhibited a mesenchymal phenotype and proliferated more actively than those in the COI xenografts. Additionally, compared with the COI tumors, the SOI tumors contained more cancer associated fibroblasts, matrix metallopeptidase 2 and 9. In conclusion, SOI is a feasible and reliable technique to establish OCOX mouse models mimicking the clinical process of ovarian cancer growth and metastasis, although SOI is more technically difficult and time-consuming than COI.

Correspondence to: Professor Zehua Wang, Department of Obstetrics and Gynecology, Union Hospital, Tongji Medical College, Huazhong University of Science and Technology, 1277 Jiefang Avenue, Wuhan 430022, P.R. China
E-mail: zehuawang@163.net

*Contributed equally

Abbreviations: OCOX, ovarian cancer orthotopic xenograft; COI, cellular orthotopic injection; SOI, surgical orthotopic implantation; PDXs, patient-derived xenografts; GEMMs, genetically engineered mouse models; DMEM/F12, Dulbecco's modified Eagle's medium: nutrient mixture F-12; GFP, green fluorescent protein; BLI, bioluminescent imaging; ROI, region of interest; MMP, matrix metallopeptidase; CAFs, cancer-associated fibroblasts; MVD, microvessel density; EMT, epithelial-mesenchymal transition; EdU, 5-ethynyl-2'-deoxyuridine; α-SMA, α-smooth muscle actin

Key words: bioluminescence measurements, metastasis, orthotopic xenograft model, ovarian cancer, tumor microenvironment

Introduction

Ovarian cancer has the highest mortality rate of all gynecologic malignancies (1), mainly because most patients present with advanced disease and widespread metastasis at the time of their diagnosis. The standard treatment strategy is surgery followed by platinum-based chemotherapy. Although the majority of patients are initially sensitive to chemotherapy, most eventually develop drug resistance or disease recurrence, resulting in treatment failure. This common outcome makes the investigation of new drugs and therapeutic modalities imperative. Appropriate animal models of ovarian cancer are required for screening drugs and preclinical studies. Positive results are often 'overpredicted' in preclinical studies, with the highly encouraging preclinical results in mouse models often failing to show efficacy in phase III clinical trials on patients with metastatic tumors (2). It is likely that this disconnect between research success and clinical outcomes is mainly because mouse models of spontaneous metastatic or advanced disease have rarely been used in such studies (2,3). Chemotherapy response varies according to a tumor's organ environment, as well as between the primary tumor and recurrent or metastatic tumors (4). Therefore, models that closely replicate the spontaneous progression of metastatic ovarian cancer are of great importance.

In studying ovarian cancer, there are four commonly used animal xenograft models based on the site of tumor transplantation: subcutaneous, intraperitoneal, subrenal capsule

and orthotopic tumors. The conventional subcutaneous tumor model is the most widely used model for screening anti-cancer drugs because the technique of subcutaneous injection is straightforward. Although the growth of subcutaneous xenografts can be easily monitored, spontaneous metastases have been seldom observed. The intraperitoneal tumor model simulates the process of peritoneal dissemination and ascites formation in ovarian cancer, and has generally been used to evaluate the efficacy of intraperitoneal chemotherapy. However, the relatively short life span of mice and the absence of primary tumors and spontaneous metastases have limited its utility. Subrenal capsule models have been used to determine the responsiveness of patient-derived xenografts (PDXs) to chemotherapeutic agents because of a high take rate (5,6). Since ovarian cancers originate in the ovary or fallopian tubes, none of the three models mentioned above can accurately reflect clinical disease progression and the therapeutic response of cancer patients.

In the orthotopic model, tumor cells or tissues are transplanted into the ovaries. By simulating the microenvironment of human ovarian cancer, this model can closely replicate the gene expression profiles, histopathologic features, clinical disease progression and interactions between cancer cells and the relevant microenvironment (7). Both primary solid tumors and spontaneous metastases exist in this model, allowing for a greater probability of clinical relevance and translation, especially in predicting subsequent results for metastatic cancer patients (8). However, despite the benefits, orthotopic models have technical difficulties and are time-consuming, and expensive, and inconvenient monitoring limit their applicability (9).

Since Fu *et al* reported the first case of PDX transplantation under the capsule of the nude mouse ovary in 1993 (10), orthotopic models of human ovarian cancer have greatly advanced in the past two decades. The rapid development of *in vivo* imaging technology has made the visual assessment of orthotopic tumors possible. So far, orthotopic ovarian cancer models can be established through the following approaches: 1) genetically engineered mouse models (GEMMs) of human-like spontaneous mouse tumors (11,12); 2) surgical orthotopic implantation (SOI) of tissue-blocks from cancer cell lines (13) or from a patient (10) implanted into the ovary of an immune-deficient mouse; and 3) an intrabursal injection of tumor cells into the ovary of an immune-deficient mouse (cellular orthotopic injection, COI) (14). GEMMs are established in immune-competent mice by editing the mouse genome through the use of transgenic technology (inserting extra DNA into the genome to encode target genes) or knockout/knock-in technology (selectively modifying specific portions of the mouse genome) (11). Thus, GEMMs are particularly suitable for assessing immune-based therapies (2,11).

Currently, the application of orthotopic xenograft tumors in ovarian cancer is less common due to the procedure's technical challenges and the expensive testing equipment required. While COI and SOI are the two most common ways of modeling orthotopic ovarian cancer, there are few studies that compare the characterizations and applicable situations for COI and SOI. In several studies of solid tumors, including bladder (15), lung (16,17), kidney (18) and pancreatic cancer (19), SOI was found to be more malignant and clinically relevant than COI. Specifically, SOI tumors were larger and much more invasive than COI tumors, and the survival time of the mice in SOI groups was shorter. Yi *et al* (20) established an orthotopic ovarian cancer mouse model using three pathways (cell suspension; cell suspension isolated from subcutaneous tumor; tissue-block from subcutaneous tumor) and concluded that a tissue-block derived transplantation model better simulated tumor development and invasion. However, the cell line used in the study was 4T1, a breast cancer cell line, which cannot actually reflect the features of ovarian cancer. Here, we conducted a head-to-head comparison of COI and SOI that derived from ovarian cancer cell lines.

In this study, we utilized continuous dynamic *in vivo* bioluminescence imaging to demonstrate the differences in tumor formation and progression between COI xenografts and SOI xenografts derived from luciferase-marked human ovarian cancer cell lines and summarize the advantages and disadvantages of these two models. We also compared the two models through cellular experiments and immunohistochemistry of the tumor samples. We believe that this study can help researchers select the appropriate mouse model for ovarian cancer research.

Materials and methods

Cell culture. The human ovarian cancer cell lines SKOV3 (a serous adenocarcinoma cell line) and ES2 (a clear cell carcinoma cell line) were obtained from American Type Culture Collection and maintained in DMEM/F12, supplemented with 10% fetal bovine serum and 1% penicillin and streptomycin. All cells were maintained at 37˚C with 5% CO_2 in a humidified incubator. Cells were collected in a logarithmic growth phase and inoculated as soon as possible.

Lentivirus transfection. Lentivirus transfection was used to establish ovarian cancer cell lines that were double-marked with green fluorescent protein (GFP) and luciferase. Briefly, cells were seeded into a 96-well plate with a quantity of 5000/well and infected with lentivirus (GenePharma, Shanghai, China) for 72 h. Then, the cells were screened with 5 μg/ml puromycin for 7 days. Subsequently, single cell-derived clones were established through serial dilution of the cells into 96-well plates.

Animals. Female Balb/c-nu/nu mice were obtained from the Beijing HFK Bioscience Co., Ltd., and housed in a specific pathogen free environment at Laboratory Animal Center, Huazhong University of Science and Technology. All the procedures were approved by the Institutional Animal Care and Use Committee at Tongji Medical College, Huazhong University of Science and Technology. All efforts were made to minimize suffering. Mice were euthanized when any of the following conditions occurred: primary tumors reached approximately 1 cm^3 (estimated through palpation); the mouse experienced significant weight loss (>20%); onset of cachexia or moribundity (such as massive ascites).

Orthotopic ovarian cancer xenografts. Female nude mice age 5-6 weeks and weighed 17-18 g were randomized into four groups: SKOV3/SOI, SKOV3/COI, ES2/SOI and ES2/

COI (8 mice/group). For the SOI group, subcutaneous tumors were established by inoculating $5x10^6$ SKOV3-luc or ES2-luc cells into the right axillary regions of 2 nude mice aged 4 weeks, and allowing growth of approximately 0.5 cm^3. The subcutaneous tumors were extracted and cut into 1 mm^3 pieces. The mice were anesthetized and placed on their right side. An 8-mm lateral dorsal incision was made into the fat pad surrounding the ovary, below the left kidney. After opening the ovarian capsule, one tissue-block was implanted on the ovary by a 7-0 surgical suture under a stereomicroscope, and then the ovary was covered using the surrounding fat tissue. Finally, the ovary was re-inserted, and then the abdomen and skin were closed with a 5-0 surgical suture.

For the COI group, *in vitro* cultured cells were re-suspended at a concentration of $5x10^5$ cells/5 μl and injected into the ovarian bursa using a 32 G syringe needle (Hamilton, Bonaduz, Switzerland).

Animal bioluminescent imaging (BLI). The BLI was conducted using an *in vivo* imaging system (IVIS, Xenogen Corp./ Caliper life Science, Alameda, CA, USA) once a week after implantation. A 150 mg/kg dose of D-Luciferin potassium salt (Perkin-Elmer, Hopkinton, MA, USA) was intraperitoneally injected into the mice 10 min before imaging. The mice were anesthetized using isoflurane and imaged dorsally. The region of interest (ROI) was selected and the radiance value was measured by Living Image® 4.3.1 Software (Caliper Life Science). At the end-point of observation, all the mice were euthanized immediately after the last *in vivo* BLI. To detect intraperitoneal metastases, abdominal organs were obtained within 5-10 min of being euthanized to perform *ex vivo* BLI.

Tumor size and immunohistochemistry. Tumor diameters were measured by a slide caliper, and the tumor volume was calculated as Volume = Length x Width x Height/2. Samples were fixed by 4% paraformaldehyde, followed by paraffin embedding.

Paraffin-embedded xenograft samples were used for the immunohistochemical staining of microenvironment-related markers, including α-smooth muscle actin (α-SMA), CD34, matrix metallopeptidase 2 (MMP2) and matrix metallopeptidase 9 (MMP9). α-SMA is a commonly used marker of cancer-associated fibroblasts (CAFs) (21). CD34 marked microvessel density (MVD) is a surrogate marker of tumor angiogenesis (22). MMP2 and MMP9 are two main members of the Zn-dependent proteases family, metalloproteinase (MMP), which can degrade tissue matrix and basal membranes, resulting in the migration of cells (23). In addition, E-cadherin and vimentin, markers of epithelia and mesenchymal cells, respectively, were assessed to evaluate the occurrence of epithelial-mesenchymal transition (EMT) in tumor cells (24).

Cell proliferation was determined by nuclear Ki67 staining. After routine deparaffinization and rehydration, paraffin sections were subjected to heat-mediated antigen retrieval utilizing pH 6.0 citrate buffer or pH 9.0 Tris-EDTA buffer according to the manufacturer's instructions of primary antibodies. The following staining procedures were performed with a rabbit Biotin-Streptavidin horseradish peroxidase detection system (SP-9001, ZSGB-BIO, Beijing, China). Primary rabbit antibodies were diluted as follows: vimentin (ab92547, Abcam, Cambridge, UK; anti-human, mouse), 1:600; E-cadherin (ab76319, Abcam; anti-human, mouse), 1:200; α-SMA (23081-1-AP, Proteintech, Wuhan, China; anti-human, mouse), 1:400; MMP2 (sc-10736, Santa Cruz Biotechnology, Inc., Santa Cruz, CA, USA; anti-human, mouse), 1:50; MMP9 (ab38898, Abcam; anti-human, mouse), 1:200; CD34 (ab81289, Abcam; anti-human, mouse), 1:400; Ki67 (ab92742, Abcam; anti-human), 1:500. Sections were counterstained with hematoxylin.

Images were acquired at a magnification of x400 and five regions were selected. Ki67 staining was presented as the percentage of positive cells (25). MVD was calculated based on CD34 staining (26). All the other markers were measured by Image-Pro Plus, version 6.0 (Media Cyberbetics, Bethesda, MD, USA) as Mean Density = Integrated Optical Density / Area of DAB staining (27).

Primary culture of tumor cells from nude mouse subcutaneous xenografts. Luciferase-marked human ovarian cancer cells were isolated from subcutaneous tumor tissues. Briefly, samples were minced into pieces of 0.1 mm^3 and incubated with 1 mg/ml collagenase type 1 on a thermostat shaker at 37˚C for 2 h. After filtration with a 200-mesh sieve, the cells were centrifuged and plated in flasks. The primary cells from early passages (1-5) were used.

Scratch assay. Scratch assay was used to compare the migration capabilities of the *in vitro* cultured tumor cells and the tumor cells primarily isolated from xenografts. The assay was performed as previous described (28). Images were captured at 0, 6, 12 and 24 h with a magnification of x40. The average distance of migration was quantified using Image-Pro Plus version 6.0. The assays were performed in triplicate and repeated at least three times.

5-Ethynyl-2'-deoxyuridine (EdU) incorporation assay. Cell proliferation was detected by EdU assay, using a Cell-Light EdU kit (Ribobio, Guangzhou, China) following the manufacturer's instructions. Images were acquired at a magnification of x100, and the percentage of EdU-positive cells was calculated. The assays were performed in triplicate and repeated at least three times.

Statistical analysis. All data are presented as the mean ± standard deviation. The differences between the two groups were analyzed by Student's t-test using SPSS version 22.0 (IBM Corp, Armonk, NY, USA). The results were considered to be statistically significant at P-values <0.05.

Results

Tumor formation and growth. Xenografts tumor formation was observed in the ovaries of all of the mice in the ES2/SOI and SKOV3/SOI groups, while the tumor formation rates in the ES2/COI and SKOV3/COI groups were 87.5% (7/8). Potential cell leakage would be detected by BLI, and identified by taking into account the surgery, cell line usage and the first BLI images. The two main situations we have encountered were: 1) in highly metastatic cell lines, signals were evenly distributed throughout the abdomen, with no significant high-light signals in the ovarian portion (Fig. 1A); and 2) in lower

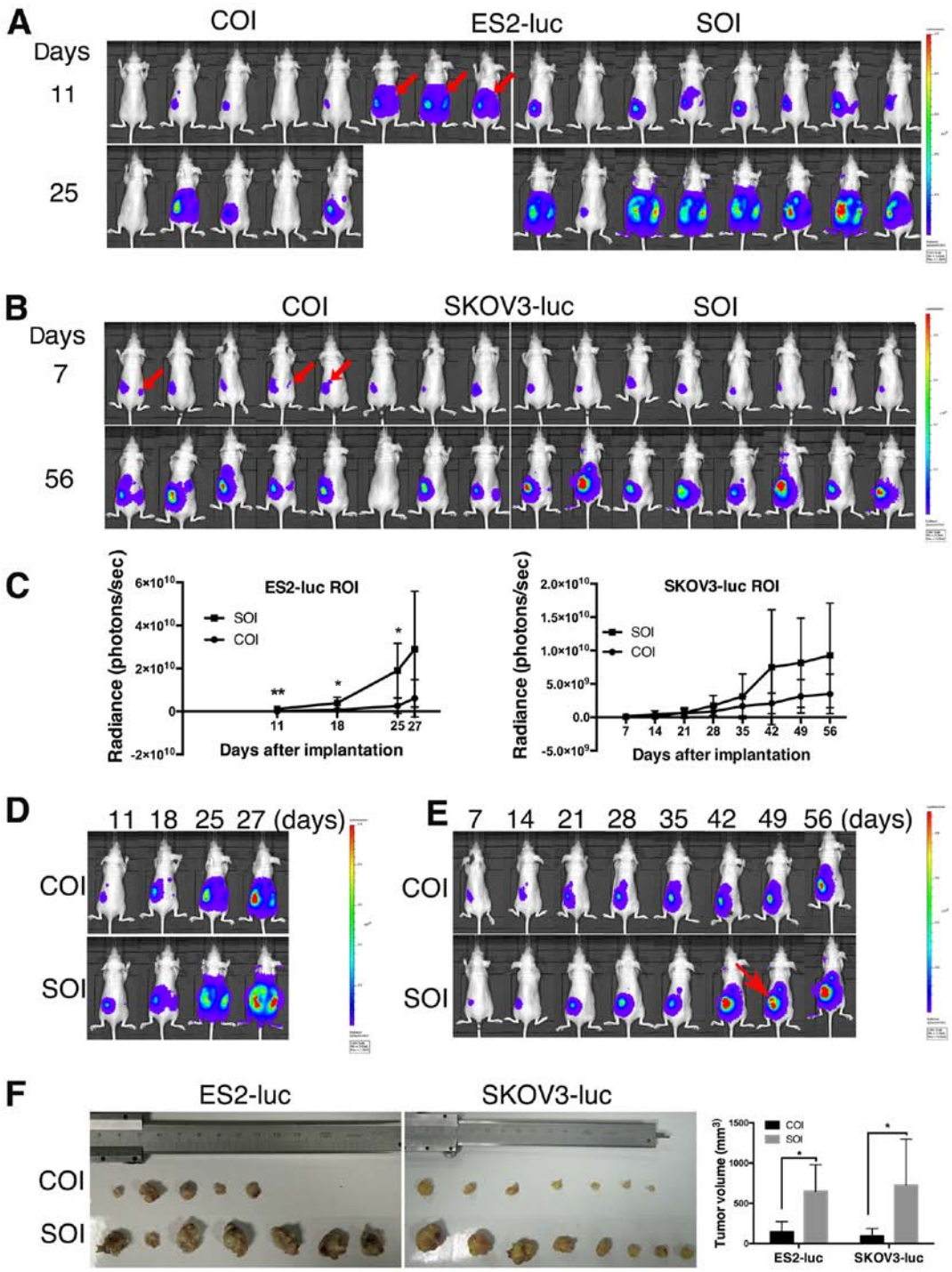

Figure 1. Tumor growth monitored by bioluminescent IVIS imaging and tumor volume. (A) BLI images of ES2-luc implanted mice. Red arrow: suspected cell leakage. (B) Images of SKOV3-luc implanted mice. Arrow: suspected cell leakage. (C) Growth curve of SKOV3-luc and ES2-luc tumors based on quantitative radiance value of IVIS imaging. (D and E) Each line of bioluminescent images represents the tumor growth of one single mouse with the strongest signal in each group. (D) ES2-luc, (E) SKOV3-luc. Red arrow: compared to the image of 42 days, it is supposed that tumor necrosis in the central region caused the signal reduction. (F) Ovarian primary tumors. Left, ES2-luc (one SOI mouse died before the last BLI); middle, SKOV3-luc; right, quantitative analysis of tumor volume. $^{*}P<0.05$; $^{**}P<0.01$.

metastatic cell lines, bioluminescent signals were outside the ovarian projection area on the body's surface (Fig. 1B). Tumor cell leakage occurred in 37.5% (3/8) of the mice in the COI groups, whereas no cell leakage was observed in the SOI groups.

The xenografts in the ES2/SOI and SKOV3/SOI groups progressed more aggressively than in the COI groups. Specifically, ES2/SOI tumors exhibited extremely rapid growth, and the mice showed a shorter survival of only 27 days. Since three cases of COI were found to have cell leakage at 11 days, and quickly progressed into a moribund state, the data from these three cases were removed during statistical analysis. One COI mouse failed to form a tumor, though BLI showed a successful injection at 7 days. COI

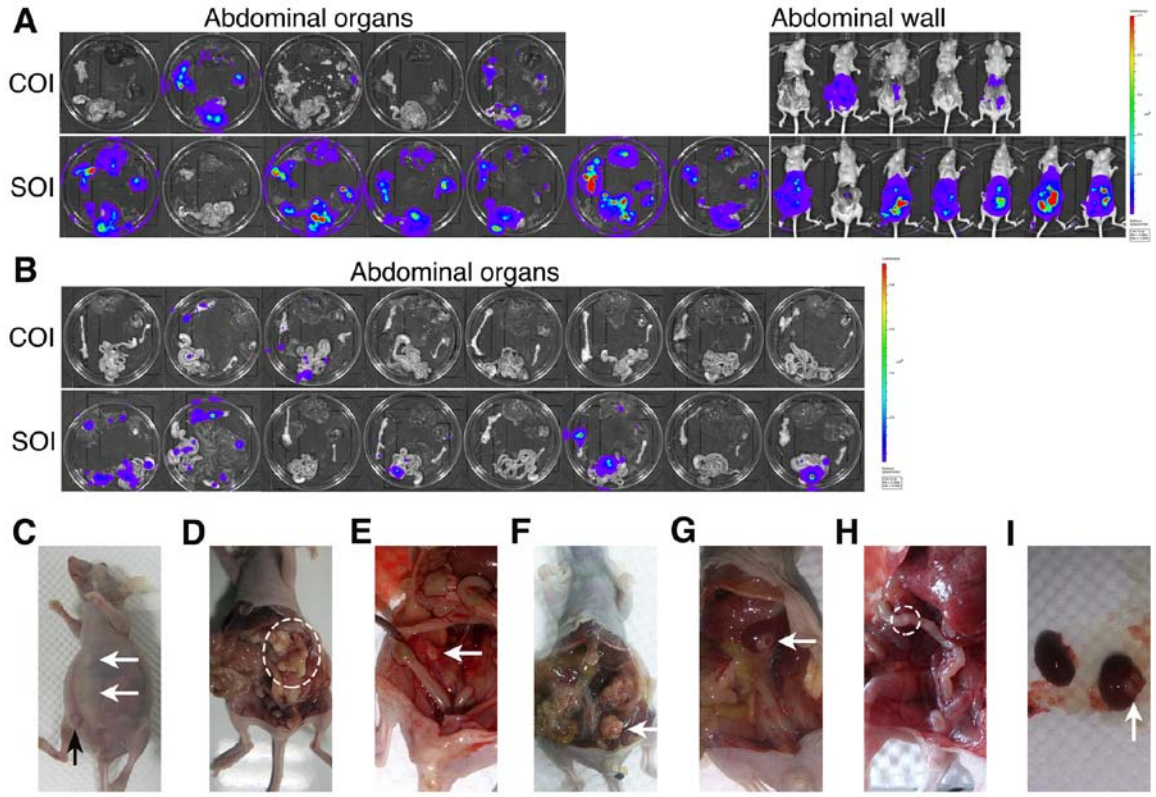

Figure 2. Comparison of intraperitoneal metastasis between COI and SOI. (A) Bioluminescent images of metastases on abdominal organs and abdominal wall in ES2-luc implanted mice. The organs arranged clockwise from the top are: liver, kidneys, intestine and mesentery, spleen with pancreas and omentum. (B) Abdominal organ (liver, kidneys, contralateral ovary, intestine and mesentery, spleen with pancreas and omentum, arranged clockwise) metastases in SKOV3-luc groups. (C-I) Photos of metastases observed in orthotopic mouse model. (C) Highly cellular and milky ascites of ES2-luc (white arrow). Black arrow: abdominal subcutaneous metastasis caused by luciferin injection during IVIS imaging. (D) Thickened omentum adheres to surrounding organs. (E) Mesenteric metastasis. (F) Metastasis on peritoneum. (G) Splenic metastasis. (H) Intestinal metastasis. (I) Renal metastasis.

xenografts showed retarded growth compared with SOI xenografts (Fig. 1A and D), and significant differences could be observed at 11 days (P=0.008), 18 days (P=0.028) and 25 days (P=0.017) (Fig. 1C).

Compared with ES2-luc, the SKOV3-luc implanted mice formed relatively slow growing tumors and were euthanized at 56 days when tumor volume was estimated to exceed 1 cm^3 by palpation. Additionally, there was one failure case in the COI group. Although not statistically significant, the bioluminescence growth curve suggested a relatively faster growing tendency in SOI tumors (Fig. 1B, C and E). Of note, through the repeated imaging of each mouse, we found one case of tumor necrosis in a SOI mouse (Fig. 1E). This may have been caused by rapid tumor growth in SOI.

The results of tumor volume showed that both ES2-luc and SKOV3-luc SOI xenografts were significantly larger than corresponding COI xenografts (P_{ES2}=0.010, P_{SKOV3}=0.018; Fig. 1F). These results suggest that tumor cells in SOI grow faster than COI and can form relatively larger primary tumors.

SOI generates xenografts of a more aggressive phenotype than COI. Consistent with the malignancy of cancer cells, ES2-derived orthotopic tumors exhibited highly metastatic properties and generated more metastases than SKOV3-luc cells *in vivo*. Three of the five COI mice (60%) and all the SOI mice (100%, 8/8) developed metastasis. Among them, ascites eventually appeared in one COI mouse and six SOI mice. By contrast, the rate of metastasis in SKOV3 group was low. Only 25% (2/8) COI mice and 62.5% (5/8) SOI mice were found to have metastases, and no formation of ascites was observed.

Moreover, we observed markedly more metastases in mice with SOI xenografts compared with the COI groups (Table I). These results were confirmed by *ex vivo* BLI analysis of removed pelvic and abdominal organs (Fig. 2A and B). Metastases spread across the abdominal cavities of the mice, including the kidney, spleen, omentum, intestine, mesentery and the abdominal wall. In addition, consistent with the progression of human ovarian cancer were the formation of ascites (Fig. 2C-I), with the omentum and mesentery the most commonly involved organs. Among mice with metastasis in the SOI groups, tumor cells mainly metastasized to the omentum (6/7 of ES2, 3/5 of SKOV3) and mesentery (5/7 of ES2, 4/5 of SKOV3). However, in COI groups, although mesentery (2/3 of ES2, 1/2 of SKOV3) was still the main target of metastasis, omentum metastasis (1/3 of ES2, 0/2 of SKOV3) was rarely observed.

The cells that generate SOI and COI xenografts are different in migration and proliferation. Having established that SOI tumors are more aggressive than COI tumors, we next investigated whether cell malignant properties are different between the tumor cells that form SOI and COI xenografts. Thus, we isolated tumor cells from subcutaneous tumors (ES2-luc-M and SKOV3-luc-M, the cells that generate SOI tumors) and compared them with those routinely *in vitro* cultured tumor

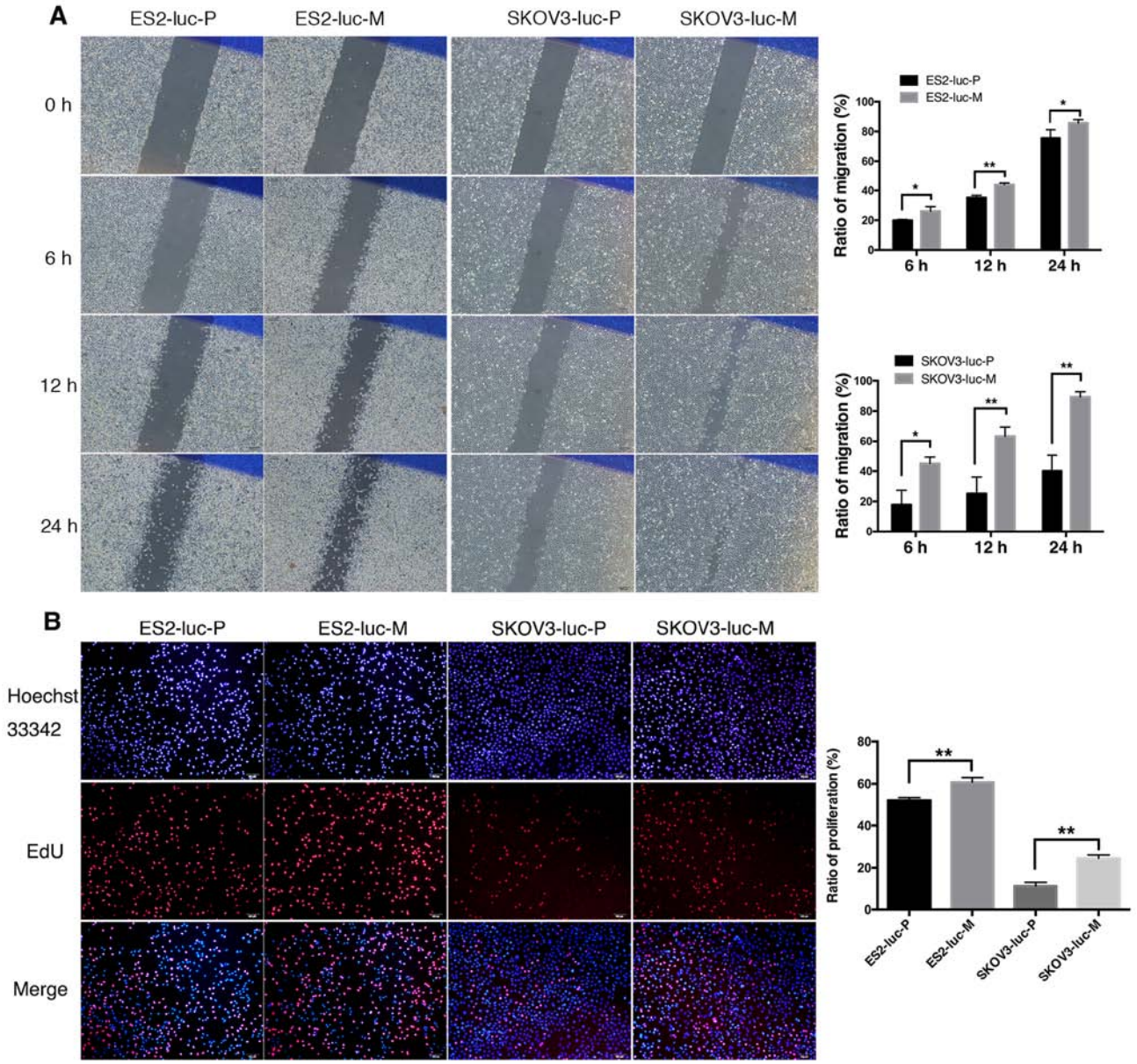

Figure 3. Primary cells from subcutaneous tumor tissue, exhibit stronger migration and proliferation capability than parental cells. (A) Scratch assay of parental cells and primary cells from mouse tumors (ES2-luc-M and SKOV3-luc-M). The right panel is quantitative assay of migration ratio. Images were captured at a magnification of x40. (B) EdU assay. Right panel: quantitative assay of proliferation ratio. Images were captured at a magnification of x100. *P<0.05; **P<0.01.

cells (ES2-luc-P and SKOV3-luc-P, the cells that generate COI tumors) in regards to migration and proliferation.

The scratch assay results showed that the primary cells of ES2-luc subcutaneous tumors have a stronger migration capability than the parental cells (Fig. 3A). Gap closure in both groups began within 6 h after the scratch, and significant differences could be observed ($P_{6\,h}$=0.029). At 12 and 24 h, the migration areas of ES2-luc-M cells were increased by 25 and 13% ($P_{12\,h}$=0.001; $P_{24\,h}$=0.047). Similar results were observed in SKOV3-luc-P/M cells. Primary cells showed significant migration at 6 h and progressed until the gap was nearly invisible at 24 h. In contrast, this process of SKOV3-luc-P cells was significantly retarded, and 60% of the initial gap still remained at 24 h. The migration areas of SKOV3-luc-M cells at 6, 12 and 24 h were 2.23-2.53-fold to the SKOV3-luc-P groups ($P_{6\,h}$=0.011; $P_{12\,h}$=0.006; $P_{24\,h}$=0.002).

In the EdU assays, significant differences in EdU-positive cell ratio were observed in both pairs of cell lines: ES2-luc-M versus ES2-luc-P, 52.0%±1.5% versus 60.7±2.2%, P=0.005; SKOV3-luc-M versus SKOV3-luc-P, 11.4±1.8% versus 24.5±1.6%, P=0.001 (Fig. 3B). These findings suggest that primary cells isolated from the subcutaneous tumors that form SOI tumors have a stronger potential for migration and proliferation.

Tumor microenvironment in SOI and COI xenografts. In a similar study of kidney cancer, it is believed that supportive stromal tissue and cell-cell communication within a tissue-block, namely the tumor microenvironment, plays an important role in the full expression of cancer cell spontaneous metastatic potential (18). Thus, we detected several tumor microenvironment and metastasis-related markers using

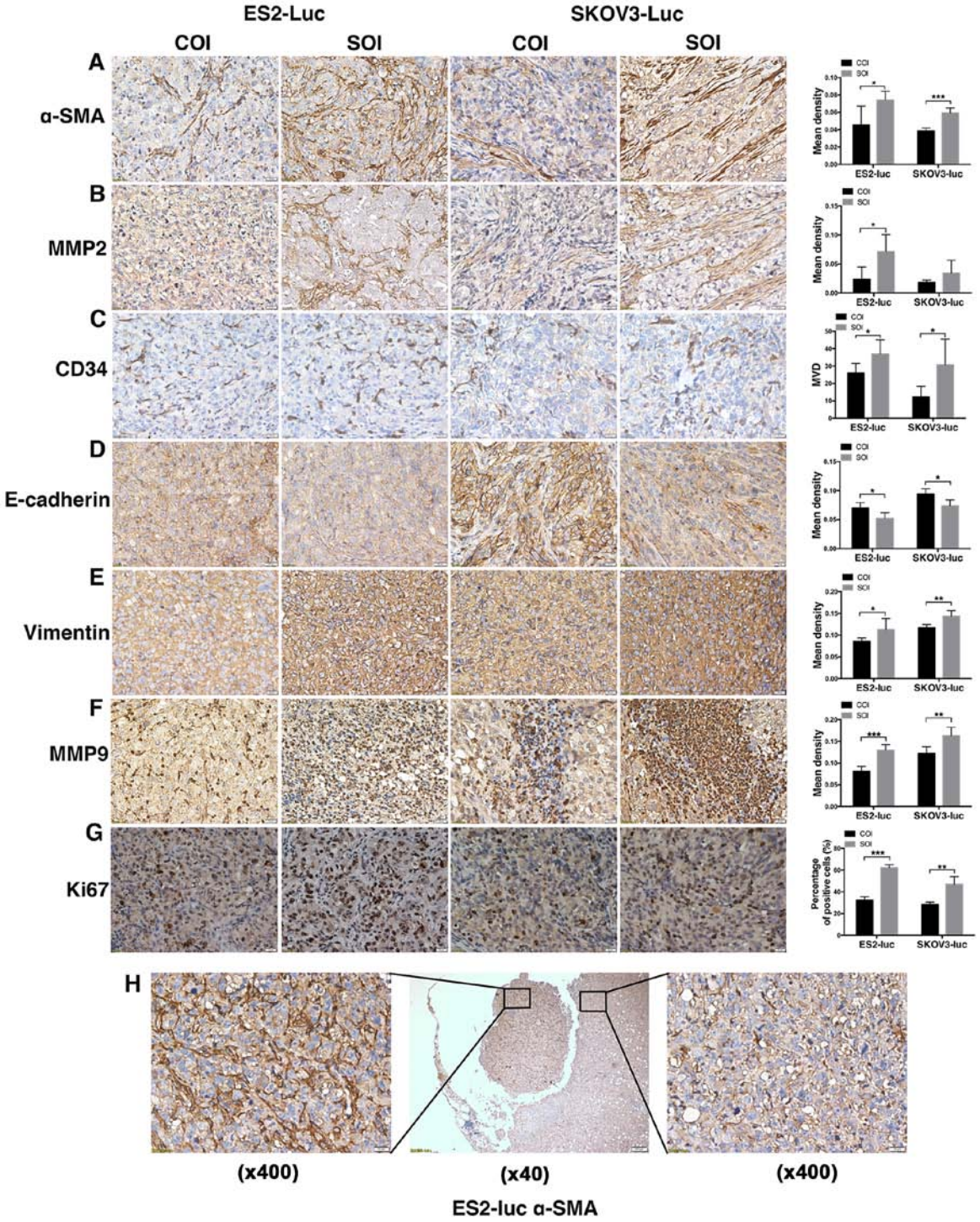

Figure 4. Immunohistochemistry of microenvironment related markers on tumor samples. (A-G) Immunostaining for α-SMA, MMP2, CD34, E-cadherin, vimentin, MMP9 and Ki67 in tumor samples. The expression of all markers in SOI tumors was more than that in COI tumors (although no statistical difference was observed for MMP2 in SKOV3-luc tumors, the mean of MMP2 mean density in SOI was higher than COI). All images were captured at a magnification of x400. (H) One piece of tumor tissue shedding from local tumor and significant difference of α-SMA expression existed between the two areas. *P<0.05; **P<0.01; ***P<0.001.

immunohistochemistry staining in the COI and SOI ovarian xenograft samples.

Positive staining of α-SMA was mainly localized to tumor stroma, and the results (P_{ES2}=0.020; P_{SKOV3}<0.001) showed that there were more CAFs in SOI tumors (Fig. 4A). CAFs can be induced by tumor cells to synthesize active MMP2 (29,30). Through MMP2 staining, we found that the localization and distribution of MMP2 were very similar to α-SMA, and MMP2's elevated expression in SOI tumors also confirmed a higher level of activation in SOI stromal fibroblasts (P_{ES2}=0.024; P_{SKOV3}=0.155; Fig. 4B). The staining of CD34 revealed that MVD of ES2-SOI group was 1.42-fold to COI group. The 2.49-fold in SKOV3 tumors also suggests an enhanced tumor angiogenesis in SOI tumors (P_{ES2}=0.049; P_{SKOV3}=0.046; Fig. 4C).

As the main markers of EMT, the expression of E-cadherin (P_{ES2}=0.017; P_{SKOV3}=0.011) and vimentin (P_{ES2}=0.046;

Table I. Metastasis of the nude mouse groups with orthotopically implanted human ovarian cancer.

Groups	Metastasis rate	Ascites	Organs						
			Omentum	Intestine and mesentery	Liver	Spleen	Kidney	Contralateral ovary	Peritoneum
ES2-luc-COI	3/5	1/5	1/5	2/5	0/5	1/5	2/5	0/5	3/5
ES2-luc-SOI[a]	8/8	6/8	6/7	5/7	3/7	5/7	5/7	0/7	7/7
SKOV3-luc-COI	2/8	0/8	0/8	1/8	0/8	1/8	0/8	0/8	2/8
SKOV3-luc-SOI	5/8	0/8	3/8	4/8	2/8	0/8	1/8	0/8	4/8

[a]Since one mouse died before the last BLI, the data of organ metastases in ES2-luc-SOI group were summarized from 7 mice.

Table II. Advantages and disadvantages of the two models.

Groups	COI	SOI
Experimental cycle length	Relatively short	Relatively long (because of subcutaneous tumor formation)
Technical requirement	Microscopic injection	Microscopic suture
Cell leakage	Easy to cause intraperitoneal dissemination	Seldom cause artificial metastasis
Transient regulation to cells[a]	Able	Unable
Take rate	Low	High
Growth speed	Slow	Rapid
Metastatic capability	Weak	Strong
Stability of tumorigenesis	Less stable	More stable

[a]Regulation at cellular level, such as cells after transient transfection and cell suspensions that contain two or more cell types.

P_{SKOV3}=0.004) indicated that SOI holds a higher level of EMT (Fig. 4D and E). Different from MMP2, as another important member of MMP family, MMP9 is mainly localized to the area of inflammatory cell infiltration, which was consistent with the theory that tumor-associated macrophages are the main source of MMP9 (31). In SOI tumors, MMP9 staining frequently exhibited large block aggregations, while the staining regions in COI tumors were rather small (P_{ES2}<0.001; P_{SKOV3}=0.006; Fig. 4F). Lastly, results of Ki67 (P_{ES2}<0.001; P_{SKOV3}=0.004) suggested a higher proliferation capability of cancer cells in SOI tumors (Fig. 4G).

Additionally, we found a piece of tumor tissue shedding from the local tumor (Fig. 4H), which was about to form metastasis. Noteworthy, there were significant differences in the expression of α-SMA between the shedding tissue and the local tissue (Fig. 4H).

Discussion

In this study, we successfully established an orthotopic ovarian cancer mouse model by injecting tumor cells (COI) or transplanting tumor tissue-blocks into the ovary (SOI). By utilizing ovarian cancer cell lines that stably express GFP and firefly luciferase, which enabled *in vivo* bioluminescent/fluorescent imaging of live tumor cells, the monitoring of tumor growth was no longer a limiting factor in the application of orthotopic xenograft models. After a series of dynamic BLI imaging, we made a comparison of tumor growth and metastasis between COI and SOI tumors and found that SOI tumors exhibited a higher take rate, faster growth and more aggressive phenotype than COI. This conclusion was consistent with previous studies (15-19).

In recent years, the application of orthotopic ovarian cancer mouse models has greatly increased, with COI and SOI the most commonly used methods. Many researchers chose to use COI, which may have been due to the relative simplicity of the procedure and its short experimental cycle (no subcutaneous tumor formation or tissue-block requirement). The take rate of orthotopic tumors varies depending on researcher experience and experimental conditions. In most studies, take rates of up to 100% were achieved, regardless of whether COI or SOI was the method used (14,32). In our study, all the orthotopic implantation surgeries were performed by the same person. The take rate in the SOI group also reached 100%, but it was only 87.5% in the COI group, even though successful injection was proved by the first BLI in all mice.

Cell leakage may result in non-spontaneous metastasis. In our study, none of the SOI mice were found to have cell leakage, while several COI mice did. We believe that the cells leak out mainly through the pinhole caused by the injection or due to an incomplete ovary capsule (if the mouse was too young). Therefore, SOI is recommended for studies of tumor metastasis, because COI may exhibit false positive results and cause experimental variability (18). When COI is the only

choice due to experimental limitations, some improvements may help to prevent cell leakage: 1) use of semi-solid medium to fix cells (33); 2) use of biological glue for closure of the pinhole; 3) the usage of relatively older mice (aged 6 weeks or more) may be helpful. Additionally, since the inoculation surgery takes a certain amount of time (approximately 10 min per mouse, according to the operator's experience and advanced equipment) and the viability of suspended cells may decrease over time in COI surgeries of a large quantity, it is better to use SOI models in this situation. In SOI surgeries, it is recommended that peripheral tissue of the subcutaneous tumor be used, which provides better viability. The advantages and disadvantages of the two models are compared in Table II.

Metastasis can be observed in almost all the studies of the orthotopic ovarian cancer model. Similar to clinical disease, peritoneal dissemination is the main pathway of metastasis. Almost all of the organs in the abdominal cavity may be involved, including the liver, spleen, kidney, mesentery, omentum and paraaortic lymph node (13,14,32). Our results of metastasis showed that SOI tumors were more metastatic than COI. Consistent with other similar studies, the incidence of abdominal wall metastasis was the highest: except for one SKOV3-SOI mouse, all the mice were found to have metastases on the surface of the peritoneum (32). In spite of the peritoneum, metastatic patterns of abdominal organs differed between COI and SOI. Omentum was one of the organs most commonly involved in SOI metastasis, while omentum metastasis was rarely observed in COI. As it is understood that the omentum is the main target organ of ovarian cancer metastasis, up to 80% of epithelial ovarian cancer patients are found to have omentum metastasis when diagnosed (34,35). This suggests that the biological characteristics of cancer cells in the SOI model are more closely related to clinical disease, thus SOI is more clinically relevant. In addition, in studying the metastasis of a particular organ, *in vivo* selection of highly metastatic cell sub-lines using the orthotopic model may help to better understand the organ selectivity of metastasis (14).

Using scratch assay and EdU assay, we confirmed that the migration and proliferation ability of cancer cells that form SOI tumors was stronger than the parental cells that form COI tumors. We think this may be due to the activation of cancer cells by stroma in the subcutaneous tumor, so we further evaluated tumor microenvironment markers in COI/SOI xenografts. Immunohistochemistry showed more CAFs (21) and a higher level of angiogenesis in SOI, indicating that the tumor microenvironment in SOI is more conducive to cell proliferation and metastasis. In a previous study of kidney cancer, the vasculature in the SOI model was also found to be richer than that in COI model (18). Elevated EMT activation and expression of Ki67 and stromal MMPs also suggested that tumor microenvironments in SOI tumors are more pro-proliferative and pro-metastatic.

In summary, through a comprehensive comparison of COI and SOI ovarian cancer modeling, we found that SOI is more malignant and clinically relevant than COI. Furthermore, the pros and cons of COI/SOI and methods of improvement were summarized. We believe this study provides useful recommendations and evidence for modeling orthotopic ovarian cancer. The SOI models can serve as useful tools for research into the metastasis and microenvironments of ovarian cancer and more accurately predict the efficacy of future clinical treatments.

Acknowledgements

We are grateful to Shunchang Zhou (Director of Laboratory Animal Center, Huazhong University of Science and Technology) for technical support. This study was supported by the National Natural Science Foundation of China (81272860, 81472443 and 81572572).

References

1. Siegel RL, Miller KD and Jemal A: Cancer statistics, 2016. CA Cancer J Clin 66: 7-30, 2016.
2. Kerbel RS: A decade of experience in developing preclinical models of advanced- or early-stage spontaneous metastasis to study antiangiogenic drugs, metronomic chemotherapy, and the tumor microenvironment. Cancer J 21: 274-283, 2015.
3. Singh M, Lima A, Molina R, Hamilton P, Clermont AC, Devasthali V, Thompson JD, Cheng JH, Bou Reslan H, Ho CC, *et al*: Assessing therapeutic responses in Kras mutant cancers using genetically engineered mouse models. Nat Biotechnol 28: 585-593, 2010.
4. Guerin E, Man S, Xu P and Kerbel RS: A model of postsurgical advanced metastatic breast cancer more accurately replicates the clinical efficacy of antiangiogenic drugs. Cancer Res 73: 2743-2748, 2013.
5. Bogden AE, Cobb WR, Lepage DJ, Haskell PM, Gulkin TA, Ward A, Kelton DE and Esber HJ: Chemotherapy responsiveness of human tumors as first transplant generation xenografts in the normal mouse: Six-day subrenal capsule assay. Cancer 48: 10-20, 1981.
6. Lee CH, Xue H, Sutcliffe M, Gout PW, Huntsman DG, Miller DM, Gilks CB and Wang YZ: Establishment of subrenal capsule xenografts of primary human ovarian tumors in SCID mice: Potential models. Gynecol Oncol 96: 48-55, 2005.
7. Céspedes MV, Casanova I, Parreño M and Mangues R: Mouse models in oncogenesis and cancer therapy. Clin Transl Oncol 8: 318-329, 2006.
8. Francia G, Cruz-Munoz W, Man S, Xu P and Kerbel RS: Mouse models of advanced spontaneous metastasis for experimental therapeutics. Nat Rev Cancer 11: 135-141, 2011.
9. Bibby MC: Orthotopic models of cancer for preclinical drug evaluation: Advantages and disadvantages. Eur J Cancer 40: 852-857, 2004.
10. Fu X and Hoffman RM: Human ovarian carcinoma metastatic models constructed in nude mice by orthotopic transplantation of histologically-intact patient specimens. Anticancer Res 13: 283-286, 1993.
11. Sharpless NE and Depinho RA: The mighty mouse: Genetically engineered mouse models in cancer drug development. Nat Rev Drug Discov 5: 741-754, 2006.
12. Howell VM: Genetically engineered mouse models for epithelial ovarian cancer: Are we there yet? Semin Cell Dev Biol 27: 106-117, 2014.
13. Kiguchi K, Kubota T, Aoki D, Udagawa Y, Yamanouchi S, Saga M, Amemiya A, Sun FX, Nozawa S, Moossa AR, *et al*: A patient-like orthotopic implantation nude mouse model of highly metastatic human ovarian cancer. Clin Exp Metastasis 16: 751-756, 1998.
14. Tamada Y, Aoki D, Nozawa S and Irimura T: Model for paraaortic lymph node metastasis produced by orthotopic implantation of ovarian carcinoma cells in athymic nude mice. Eur J Cancer 40: 158-163, 2004.
15. Fu XY, Theodorescu D, Kerbel RS and Hoffman RM: Extensive multi-organ metastasis following orthotopic onplantation of histologically-intact human bladder carcinoma tissue in nude mice. Int J Cancer 49: 938-939, 1991.
16. Wang X, Fu X and Hoffman RM: A patient-like metastasizing model of human lung adenocarcinoma constructed via thoracotomy in nude mice. Anticancer Res 12: 1399-1401, 1992.
17. Wang X, Fu X, Kubota T and Hoffman RM: A new patient-like metastatic model of human small-cell lung cancer constructed orthotopically with intact tissue via thoracotomy in nude mice. Anticancer Res 12: 1403-1406, 1992.
18. An Z, Jiang P, Wang X, Moossa AR and Hoffman RM: Development of a high metastatic orthotopic model of human renal cell carcinoma in nude mice: Benefits of fragment implantation compared to cell-suspension injection. Clin Exp Metastasis 17: 265-270, 1999.

19. Morioka CY, Saito S, Ohzawa K and Watanabe A: Homologous orthotopic implantation models of pancreatic ductal cancer in Syrian golden hamsters: Which is better for metastasis research - cell implantation or tissue implantation? Pancreas 20: 152-157, 2000.
20. Yi C, Zhang L, Zhang F, Li L, Ling S, Wang X, Liu X and Liang W: Methodologies for the establishment of an orthotopic transplantation model of ovarian cancer in mice. Front Med 8: 101-105, 2014.
21. Tommelein J, Verset L, Boterberg T, Demetter P, Bracke M and De Wever O: Cancer-associated fibroblasts connect metastasis-promoting communication in colorectal cancer. Front Oncol 5: 63, 2015.
22. Uzzan B, Nicolas P, Cucherat M and Perret GY: Microvessel density as a prognostic factor in women with breast cancer: A systematic review of the literature and meta-analysis. Cancer Res 64: 2941-2955, 2004.
23. Coussens LM, Fingleton B and Matrisian LM: Matrix metalloproteinase inhibitors and cancer: Trials and tribulations. Science 295: 2387-2392, 2002.
24. Micalizzi DS, Farabaugh SM and Ford HL: Epithelial-mesenchymal transition in cancer: Parallels between normal development and tumor progression. J Mammary Gland Biol Neoplasia 15: 117-134, 2010.
25. Xu B, Jin Q, Zeng J, Yu T, Chen Y, Li S, Gong D, He L, Tan X, Yang L, *et al*: Combined tumor- and neovascular-'dual targeting' gene/chemo-therapy suppresses tumor growth and angiogenesis. ACS Appl Mater Interfaces 8: 25753-25769, 2016.
26. Zhang Y, Tang H, Cai J, Zhang T, Guo J, Feng D and Wang Z: Ovarian cancer-associated fibroblasts contribute to epithelial ovarian carcinoma metastasis by promoting angiogenesis, lymphangiogenesis and tumor cell invasion. Cancer Lett 303: 47-55, 2011.
27. Pei J, Fu W, Yang L, Zhang Z and Liu Y: Oxidative stress is involved in the pathogenesis of Keshan disease (an endemic dilated cardiomyopathy) in China. Oxid Med Cell Longev 2013: 474203, 2013.
28. Zhu Y, Cai L, Guo J, Chen N, Yi X, Zhao Y, Cai J and Wang Z: Depletion of Dicer promotes epithelial ovarian cancer progression by elevating PDIA3 expression. Tumour Biol 37: 14009-14023, 2016.
29. Torng PL, Mao TL, Chan WY, Huang SC and Lin CT: Prognostic significance of stromal metalloproteinase-2 in ovarian adenocarcinoma and its relation to carcinoma progression. Gynecol Oncol 92: 559-567, 2004.
30. Hassona Y, Cirillo N, Heesom K, Parkinson EK and Prime SS: Senescent cancer-associated fibroblasts secrete active MMP-2 that promotes keratinocyte dis-cohesion and invasion. Br J Cancer 111: 1230-1237, 2014.
31. Huang S, Van Arsdall M, Tedjarati S, McCarty M, Wu W, Langley R and Fidler IJ: Contributions of stromal metalloproteinase-9 to angiogenesis and growth of human ovarian carcinoma in mice. J Natl Cancer Inst 94: 1134-1142, 2002.
32. Yi XF, Yuan ST, Lu LJ, Ding J and Feng YJ: A clinically relevant orthotopic implantation nude mouse model of human epithelial ovarian cancer - based on consecutive observation. Int J Gynecol Cancer 15: 850-855, 2005.
33. Xu X, Ayub B, Liu Z, Serna VA, Qiang W, Liu Y, Hernando E, Zabludoff S, Kurita T, Kong B, *et al*: Anti-miR182 reduces ovarian cancer burden, invasion, and metastasis: An in vivo study in orthotopic xenografts of nude mice. Mol Cancer Ther 13: 1729-1739, 2014.
34. Nieman KM, Romero IL, Van Houten B and Lengyel E: Adipose tissue and adipocytes support tumorigenesis and metastasis. Biochim Biophys Acta 1831: 1533-1541, 2013.
35. Lungchukiet P, Sun Y, Kasiappan R, Quarni W, Nicosia SV, Zhang X and Bai W: Suppression of epithelial ovarian cancer invasion into the omentum by 1α,25-dihydroxyvitamin D3 and its receptor. J Steroid Biochem Mol Biol 148: 138-147, 2015.